Laser and Particle Beams (2016), *34*, 742–747.
© Cambridge University Press, 2016 0263-0346/16
doi:10.1017/S0263034616000707

Energy spectrum analysis for intense pulsed electron beam

J. SHEN,[1,2] H.H. AN,[3] H.Y. LIU,[4] G.E. REMNEV,[5] A.V. NASHILEVSKIY,[5] D.Y. LI,[1,2] J. ZHANG,[1,2] H.W. ZHONG,[1,2] X.J. CUI,[1,2] G.Y. LIANG,[1,2] M. QU,[6] S. YAN,[6] X.F. ZHANG,[1,2] G.L. ZHANG,[1,2] X. YU,[1,2] AND X.Y. LE[1,2]

[1]School of Physics and Nuclear Energy Engineering, Beihang University, Beijing 100191, China
[2]Beijing Key Laboratory of Advanced Nuclear Energy Materials and Physics, Beihang University, Beijing 100191, China
[3]Shanghai Institute of Laser plasma, China Academy of Engineering Physics, Shanghai 201800, China
[4]Shanghai Institute of Optics and Fine Mechanics, Chinese Academy of Science, Shanghai 201800, China
[5]Laboratory No.1, National Research Tomsk Polytechnic University, Tomsk 634050, Russia
[6]Institute of Heavy Ion Physics, Peking University, Beijing 100871, China

(RECEIVED 13 August 2016; ACCEPTED 10 October 2016)

Abstract

As the energy spread of intense pulsed electron beams (IPEB) strongly influences the irradiation effects, it has been of great importance to characterize the IPEB energy spectrum. With the combination of Child–Langmuir law and Monte Carlo simulation, the IPEB energy spectrum has been obtained in this work by transformation from the accelerating voltage applied to the diode. To verify the accuracy of this simple algorithm, a magnetic spectrometer with an imaging plate was designed to test the IPEB energy spectrum. The measurement was completed with IPEB generated by explosive emission electron diode, the pulse duration, maximum electron energy, total beam current being 80 ns, 450 keV, and 1 kA, respectively. The results verified the reliability of the above analysis method for energy spectrum, which can avoid intercepting the beam, and at the same time significantly improved the energy resolution. Some calculation and experimental details are discussed in this paper.

Keywords: Intense pulsed electron beam; Energy spectrum; Monte Carlo simulation; Magnetic spectrometer; Imaging plate

1. INTRODUCTION

Intense pulsed electron beam (IPEB) has been a hot topic for research and application during the past several decades. Generated from explosive emission diode with a typical accelerating voltage at hundreds of keV, IPEB is usually characterized by ultra-short pulse duration (~100 ns), total beam current over 1 kA, and high instantaneous power density. This can induce a rapid temperature rise and even phase change by energy deposition. Therefore, the applications of IPEB in various fields have been intensively reported, such as metal surface modification (Gao *et al.*, 2007; Hao *et al.*, 2010; Zhang *et al.*, 2011, 2013), water sterilization (Bly, 1979; Urazbahtina *et al.*, 2004), film deposition (Liu *et al.*, 2005; Cai *et al.*, 2014), and nanopowder synthesis (Kholodnaya *et al.*, 2014). Generally speaking, the energy spectrum of IPEB is of great necessity, which can help obtain the exact energy distribution in different materials, evaluate the irradiation effect, and thus optimize the beam parameter.

For the measurement of the electron beam energy spectrum, multiple diagnostic techniques can be utilized. Scintillation detectors coupled with multichannel analyzers are more likely to be given priority for their high temporal response in various cases (Wohn *et al.*, 1972). However, even if the glazed scintillator surface could survive in the IPEB irradiation, a much higher allowable counting rate is required for the large beam intensity of IPEB up to 200 A/cm^2. Furthermore, the harsh electromagnetic pulse environment of intense pulsed charged particle beams will inevitably bring difficulty to the production of signals with high signal-to-noise ratio and its stable propagation. Therefore, to avoid these problems, photographic plates (Kawai *et al.*, 1983) and phosphor screens (Cizmar *et al.*, 2007) have been chosen as the particle capture medium in magnetic spectrometer analyzers. Worth to mention, imaging plate (IP) is one kind of phosphor screens, which is capable to store spatial distribution images of the stimulating particles, such as X ray or electrons (Tanaka *et al.*, 2005). Because of its broad dynamic energy range,

Address correspondence and reprint requests to: X.Y. Le, School of Physics and Nuclear Energy Engineering, Beihang University, Beijing 100191, China. E-mail: xyle@buaa.edu.cn

https://doi.org/10.1017/S0263034616000707 Published online by Cambridge University Press

excellent recoverability, linearity, and sensitivity, as a substitute for X-ray film, IP has been used recently in a variety of applications, including electron microscopy and thermal neutron imaging (Izumi *et al.*, 2006).

This work is intended to characterize the energy spectrum of IPEB, which has an intrinsic instability from pulse to pulse. Because of that, it is important to monitor the beam parameter state in its application. All the above diagnostic methods need to intercept the beam, which makes them unavailable in the IPEB energy spectrum online measurement. To achieve this aim, a simple algorithm was proposed in this work to unfold the energy spectrum based on the diode accelerating voltage. Afterwards, to verify the reliability of this method, a magnetic spectrometer coupled with an IP was applied to experimentally obtain the energy spectrum.

2. IPEB GENERATION

This work was carried out on Beihang Intense Pulsed PAticle Beams (BIPPAB-450) accelerator (Yu *et al.*, 2015). As demonstrated in Figure 1, BIPPAB-450 accelerator uses a magneto generator to generate high-voltage pulse up to 250 keV. Rectified by a water-filled Blumlein double forming line (DFL), the pulse with 80 ns duration [full width at half maximum (FWHM)] gets a doubled voltage magnitude from an oil-filled auto-transformer.

The IPEB diode shown in Figure 2 is coupled to the front high-voltage system after insulator. When the high-pulsed negative voltage is applied to the 45 mm-diameter graphite cathode, dense plasma is formed in the ecton process on the cathode surface (Mesyats, 1995). After the electrons in the plasma get accelerated by the high pulsed voltage, IPEB is thus generated in the cathode–anode gap. It is inevitable that before the final application, IPEB needs to pass through a 50-μm-thick titanium foil anode, which is fixed and supported by a honeycomb metal grid with a transparency over 95%.

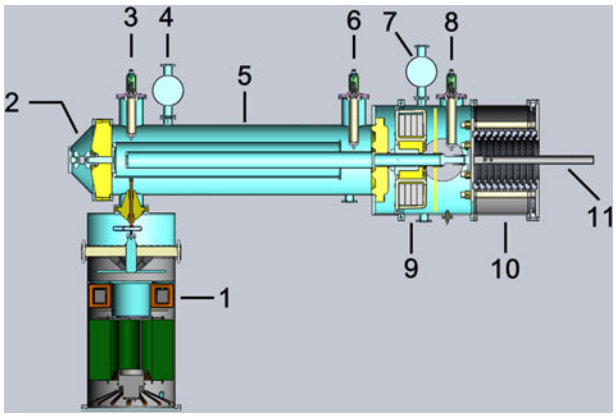

Fig. 1. Schematic diagram of BIPPAB-450 high-voltage system: 1. Magneto pulse generator, 2. Pseudospark, 3,6,8. Voltage dividers, 4,7. Observation window, 5. DFL, 9. Auto-transformer, 10. Insulator, 11. High-voltage lead.

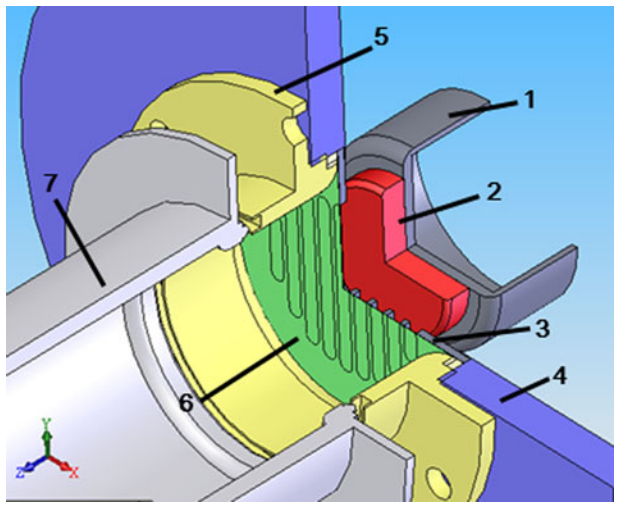

Fig. 2. Schematic diagram of BIPPAB-450 IPEB diode: 1. Cathode holder, 2. Graphite cathode, 3. Support grid, 4. Vacuum flange, 5. Anode foil sealing, 6. Titanium anode, 7. Drift chamber.

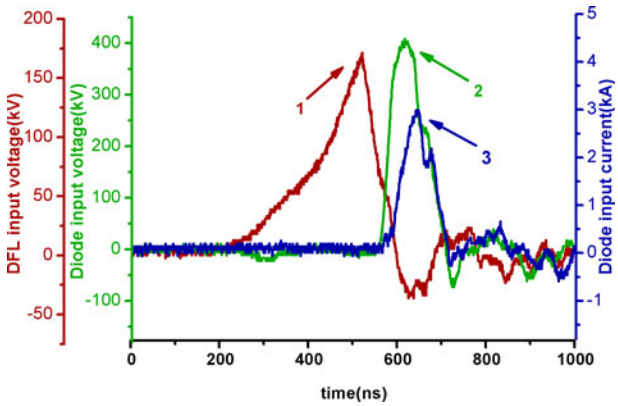

Fig. 3. Typical waveforms of IPEB generated from BIPPAB-450 accelerator: 1. DFL input voltage, 2. Diode input voltage, 3. Diode input current.

Three typical waveforms of IPEB parameters are presented in Figure 3. The voltage signals were captured with two voltage dividers and the current signal was sensed by a Rogowski coil. All of them were recorded by a Tektronix TDS 2024 oscilloscope. Worth to mention, comparing the input voltages of DFL and diode, the rectification effect of DFL to the pulse duration and the doubling effect of auto-transformer to the voltage magnitude are both well reflected. Moreover, there is a common characteristic of these three signals. Their measurements can be accomplished online without intercepting IPEB, which indicates that it can be beneficial if the relationship between the IPEB energy spectrum and any of them can be built.

3. THEORETICAL ALGORITHM

As has been stated above, in order to obtain the IPEB energy spectrum without intercepting the beam, the relative counts of electrons with various energies have to be calculated. It

https://doi.org/10.1017/S0263034616000707 Published online by Cambridge University Press

is not difficult to think of the Child–Langmuir law, which just connects the electron energy and emitted beam current:

$$J(U) = \frac{4\varepsilon_0\sqrt{2e}}{9\sqrt{m_e}} \cdot \frac{U^{3/2}}{d^2}, \quad (1)$$

where U is the accelerating voltage, d is the anode–cathode distance, ε_0 is the vacuum permittivity, e is the magnitude of the electron charge, and m_e is the electron mass.

Originally proposed by Child for the case of ions (Child, 1911) and extended to the case of electron currents between cylindrical cathodes and anodes (Langmuir, 1913), this equation should be valid for the case of IPEB as the following three assumptions are satisfied:

1. The electrons should travel between the cathode and anode, that is, no electron scattering occurs. This is equivalent to the requirement of a good vacuum in the cathode–anode gap.
2. In the anode–cathode gap, the space-charge effect of the electrons can be neglected.
3. The magnitude of the electron speed before being accelerated should be zero.

The relationship between the accelerating voltage and emitted beam current is thus established. To calculate the beam fluxes at different energies, the emitted beam current should be integrated over the time duration when the diode is working at a specific energy as below:

$$I(U_i) = \int J_i dt = \int J(U_i) dt, \quad (2)$$

where U_i denotes a specific energy, J_i is the corresponding beam current, and I is the total flux at this specific energy.

In practice, the accelerating voltage was recorded in steps of 0.4 ns, which can be treated as a differential time duration Δt. Assuming the diode works at one specific energy at one Δt, that is, it produces mono-energetic IPEB during every 0.4 ns, Eq. (2) can be rewritten in an additive form:

$$\mathrm{I}(U_i) = \sum_1^{n_i} (J_i \times \Delta t) = \sum_1^{n_i} [J(U_i) \times \Delta t] = n_i \times \Delta t \times J(U_i), \quad (3)$$

where n_i is the counts of Δt when the accelerating voltage works at the specific energy U_i. Up to now, the energy spectrum of the emitted IPEB from the diode can be obtained.

However, it should be taken into consideration that a titanium foil is placed into the propagation path of IPEB before its application on the target materials (see Fig. 2). As the foil is utilized as the anode, it is inevitable for IPEB to penetrate it. Generally speaking, electron beam will lose a part of its energy during this process, and thus energy straggling will take place as well.

Therefore, Monte Carlo simulation should be applied to simulate IPEB penetrating the titanium foil anode and finally unfold the IPEB energy spectrum. In this work, EGSnrc (Rogers *et al.*, 2010) and Fluka (Ferrari *et al.*, 2005) were chosen to complete this job. EGSnrc is open professional Monte Carlo software developed by the National Research Council Canada to model the passage of electrons and photons through matter. It can run on various system platforms. Fluka is an integrated particle physics Monte Carlo simulation open package for calculations of protons or electrons transport and interactions with matter. It can only run on the Linux or Unix system. Considering the energy range and physical model, both of them are applicable for IPEB simulation with proper setup.

4. EXPERIMENT MEASUREMENT

To verify the algorithm and acquire a solid knowledge of IPEB energy spectrum, a magnetic spectrometer was designed as shown in Figure 4. To record the electrons distribution after moving half a circle driven by Lorentz force, an IP was placed perpendicular to the incident direction of IPEB at the side of the 1 mm-diameter collimator hole. The IP consists of four layers: a protection layer (10 μm), a photostimulable phosphor layer (~100 μm), a polyester supporting layer and a metal substrate. The photostimulable phosphor layer is BaFX: Eu^{2+} (X = Cl, Br, or I, typically $Br_{0.85}I_{0.15}$) cubic crystal mixed with organic resin as a binder. IP's working principle can be simply summarized as below: IPEB can excite electron–hole pairs in the crystal. Some of the pairs recombined immediately and the rest were trapped by stable electron–hole trapping centers in the crystal. For data acquisition, He–Be laser light (632.8 nm) was used to excite the trapped carriers and their recombination can be read out as emission of blue light (~390 nm).

The magnetic field was directed perpendicularly inside the screen, and its flux intensity can be considered as 600 ± 10 Gs by calibration, with uniformity better than 2%. The magnetic spectrometer was connected to BIPPAB-450 accelerator through the drift chamber. It shared the same vacuum system with the accelerator, and thus the vacuum inside the whole chamber could reach about 0.02 Pa. In this case, no

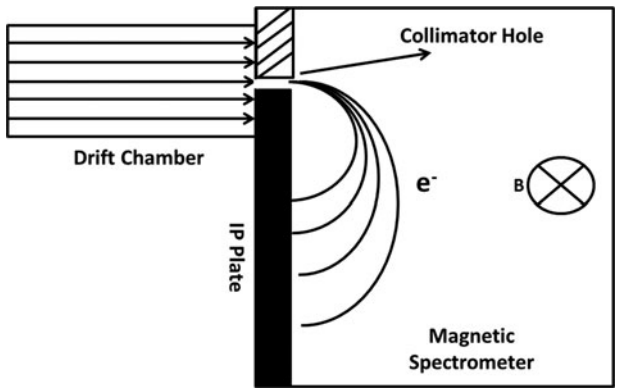

Fig. 4. Schematic diagram of magnetic spectrometer couple with IP.

https://doi.org/10.1017/S0263034616000707 Published online by Cambridge University Press

heavy air pressure was exerted on the anode foil, which could help avoid anode fracture, gas leakage, and pump damage.

After readout from IP, the information of detailed location and beam intensity can be obtained. As the speed of 400 keV electron has been closed enough to light speed, relativistic effect has to be taken into consideration. According to the relativity theory,

$$T = \left[c^2 e^2 (B\rho)^2 + m_e^2 c^4\right]^{1/2} - m_e c^2, \tag{4}$$

where T denotes the kinetic energy of electrons, c, B, and ρ are the light speed, magnetic flux intensity, and track radius, respectively. With this equation, the location data read out from the IP can be transformed into energy data. But the induced error should be taken into consideration as well, which will be discussed later.

5. RESULTS AND DISCUSSION

Figure 5 demonstrates the energy-normalized energy spectrum of IPEB before penetrating the titanium foil anode. It can be indicated from the two peaks that IPEB from BIPPAB-450 accelerator is mainly composed of electrons within two energy intervals. The relative energy fluctuations $\Delta E/E$ for these two intervals are both about 10%, which hints the same possible origin of these two peaks.

As the spectrum was calculated from the waveform of accelerating voltage with Eq. (3), the data points near the two peaks correspond to larger n_i, that is, the IPEB diode works at the specific energy U_i for a longer time. When evaluating the error, n_i and Δt are considered as constants for a specific energy U_i, and $J(U_i)$ is the only source of error. According to Eq. (1), only the error of U_i should be taken into account for $J(U_i)$, and it keeps the same for various magnitudes of energies. Considering comprehensively, n_i is the only variable that can affect the errors for different energies. That is why the data points closed to the two peaks are assigned with larger error values.

The effect of the titanium foil anode taken into account, the Monte Carlo simulation results from EGSnrc and Fluka are present in Figure 6. Comparing them with the spectrum in Figure 5, several remarkable differences can be readily figured out. Firstly, the energy magnitudes of the two peaks became a little smaller due to the energy loss in the titanium foil. Except for that, another dominating effect of the foil to IPEB is energy straggling, which can be reflected by the following details. It can be evaluated that the relative energy fluctuation $\Delta E/E$ increased significantly to almost 15%. Moreover, the two peak values of the energy-normalized intensity decreased. The last but not least one, is that a platform of electron distribution between the two peaks was formed, and its averaged energy-normalized intensity value is around half of the low-energy peak intensity. Obviously, its formation is just the sum of the right-side tail of the low-energy peak and left-side tail of the big peak. Up to now, the general energy spectrum of IPEB from BIPPAB-450 accelerator was obtained theoretically basing on the accelerating voltage. The whole process was successfully conducted without intercepting the beams. Next it becomes of great necessity to get the IPEB energy spectrum experimentally for verification.

The IPEB energy spectrum was measured with magnetic spectrometer, which has been introduced above, and the result was recorded by an IP. After data readout, the energy distribution can be intuitively recognized from the raw data as shown in Figure 7. The data contain the information of relative number of excited electron–hole pairs and corresponding location. According to Eq. (4), the location can be connected to electron energy. In this way, the IPEB energy spectrum can be experimentally obtained (see Fig. 8).

Because IP has very high spatial resolution, that is, the energy spectrum recorded by IP has very high-energy resolution as well, which can be found out if comparing Figure 8 with the calculated results in Figure 6; and some similarities of the theoretical and experimental energy spectra can be

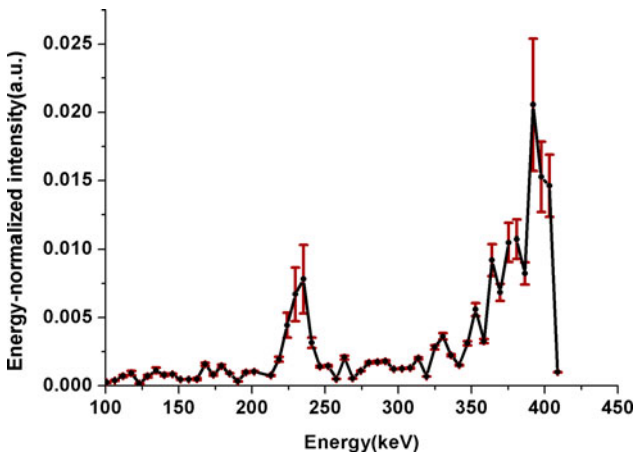

Fig. 5. Energy spectrum of IPEB after emission before penetrating the Ti anode foil.

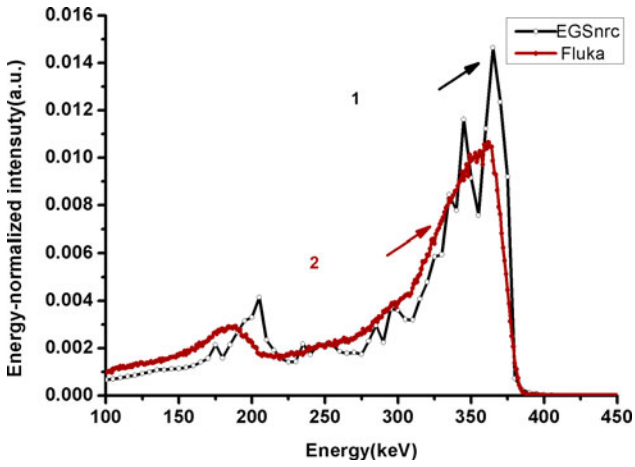

Fig. 6. Calculated energy spectrum of IPEB after passing through the Ti anode foil by: 1. EGSnrc and 2. Fluka.

https://doi.org/10.1017/S0263034616000707 Published online by Cambridge University Press

Fig. 7. Raw data of IPEB energy spectrum on IP.

figured out, such as the general shape, relative energy-normalized intensities of two peaks and the platform, relative energy fluctuation $\Delta E/E$ for two peaks. In some extent, the conformance of these parameters can already testify the applicability of the algorithm for IPEB energy spectrum evaluation. However, if looking into the detail, the energy values of the two peaks are slightly differed. The high- and low-energy peaks are located at 185, 325 keV (experiment); 180, 350 keV (Fluka); and 200, 355 keV (EGSnrc), respectively. To understand this situation, an error evaluation was made for the relativistic revision. As can be seen in Eq. (4), the errors induced by the magnetic flux intensity B and track radius ρ should be taken into consideration. According to the basic statistical idea of absolute error propagation, the IPEB energy uncertainty can be obtained with:

$$\Delta T = \frac{\partial T}{\partial B}\Delta B + \frac{\partial T}{\partial \rho}\Delta\rho = \frac{c^2e^2\rho^2 B}{(T + m_e c^2)}\Delta B + \frac{c^2e^2B^2\rho}{(T + m_e c^2)}\Delta\rho, \quad (5)$$

where ΔB and $\Delta\rho$ denote the absolute errors of the magnetic flux intensity B and track radius ρ, respectively; and to simplify the analysis, the former takes the value of maximum variation of flux intensity 10 Gs, while the latter takes the value of the collimator radius 0.5 mm. In this way, the obtained theoretical error curve for the magnetic analyzer is demonstrated in Figure 9, from which we can deduce to some extent the mechanism of the peak dislocation. The accuracy limitation of the magnetic analyzer determined that a measurement result within a relative error tolerance interval about 10% is acceptable. If examining the theoretical algorithm as a measuring method, its result is acceptable as well. Considering the real IPEB energy spectrum can

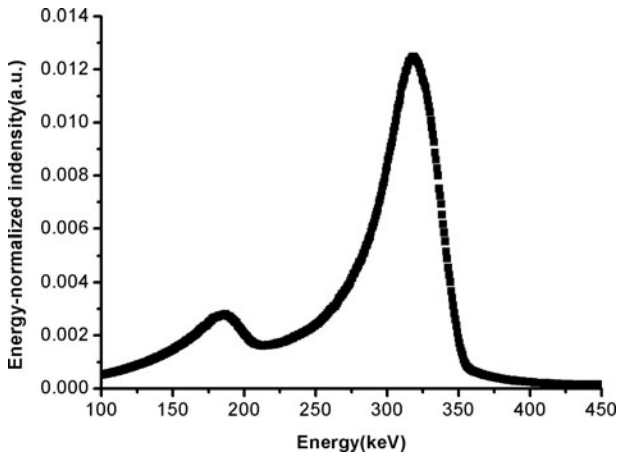

Fig. 8. Energy spectrum of IPEB read out from IP after relativistic correction.

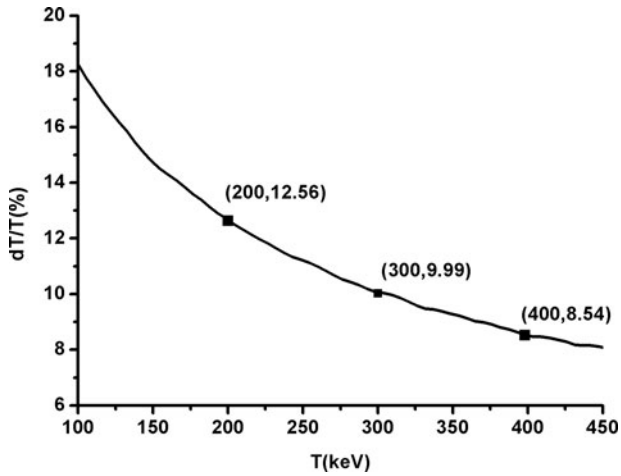

Fig. 9. Theoretical error curve of the magnetic analyzer with three labeled reference data points.

hardly be obtained, either the theoretical or experimental spectrum has been closed to the real one.

Up to now, the IPEB energy spectrum has been unfolded, while the formation mechanism of its shape with two peaks still remains unknown. To figure it out, the accelerating voltage in Figure 3 should be examined with extreme caution. It is not difficult to find out on the right side of the main peak, there is a small peak, which corresponds to the low-energy peak in the spectrum if compare their energy values. Between the main peak and the small peak there is a time delay about 40 ns. The speed for electromagnetic wave propagation in steel is about 2.7×10^8 m/s, that is, voltage signal can be propagated over a length about 10.8 m during 40 ns. That is almost twice of accelerator length. Hinted by the data, the occurrence of signal reflection due to impedance mismatch between IPEB diode and previous high-voltage system can be determined. Considering the signal propagation length and basic principles, DFL should be the exact scene where it occurred. This result can be taken for reference if one wants to reshape the IPEB energy spectrum for some specific purposes, for example, to obtain a mono-energetic beam.

6. CONCLUSION

IPEB energy spectrum was emphatically studied in this work. Basing on the accelerating voltage of IPEB diode, which can be obtained by a voltage divider without intercepting the beam, an algorithm was proposed to unfold the IPEB energy spectrum. Firstly, Child–Langmuir law was applied to build the relationship between the accelerating voltage and diode-emitted electron spectrum. Afterwards, Monte Carlo simulation with

https://doi.org/10.1017/S0263034616000707 Published online by Cambridge University Press

Fluka and EGSnrc programs was made to take the titanium anode foil into consideration. The results revealed that the energy loss and energy straggling are the two most important effects made by the foil.

A magnetic analyzer coupled with an IP was utilized to measure the IPEB energy spectrum. By comparison, the experimental results verified the applicability of the proposed algorithm for IPEB energy spectrum. And detailed analysis hinted the formation mechanism of the double-peak-shape IPEB spectrum. In perspective, this algorithm can be beneficial for beam monitoring and parameter optimization, and it can also be utilized for the charged particles with parameters in a much wider range.

ACKNOWLEDGMENTS

This work was supported by the National Natural Science Foundation of China (grant no. 11175012) and National Magnetic Confinement Fusion Program (grant no. 2013GB109004).

REFERENCES

Bly, J.H. (1979). Electron beam sterilization technology. *Radiat. Phys. Chem*. **14**, 403–414.

Cai, J., Guan, Q., Hou, X., Wang, Z., Su, J., & Han, Z. (2014). Isothermal oxidation behaviour of thermal barrier coatings with CoCrAlY bond coat irradiated by high-current pulsed electron beam. *Appl. Surf. Sci*. **317**, 360–369.

Child, C.D. (1911). Discharge from hot cao. *Phys. Rev.* (*Ser. I*) **32**(5), 492–511.

Cizmar, P., Müllerová, I., Jacka, M., & Pratt, A. (2007). New multichannel electron energy analyzer with cylindrically symmetrical electrostatic field. *Rev. Sci. Instrum*. **78**, 053714.

Ferrari, A., Sala, P.R., Fassò, A., & Ranft, J. (2005). Fluka:a multi-particle transport code. CERN-2005-10, INFN/TC_05/11, SLAC-R-773.

Gao, B., Hao, S., Zou, J., Wu, W., Tu, G., & Dong, C. (2007). Effect of high current pulsed electron beam treatment on surface microstructure and wear and corrosion resistance of an AZ91HP magnesium alloy. *Surf. Coat. Technol*. **201**(14), 6297–6303.

Hao, Y., Gao, B., Tu, G.F., Li, S.W., Hao, S.Z., & Dong, C. (2010). Surface modification of Al–20Si alloy by high current pulsed electron beam. *Appl. Surf. Sci*. **257**(9), 3913–3919.

Izumi, N., Snavely, R., Gregori, G., Koch, J.A., Park, H.S., & Remington, B.A. (2006). Application of imaging plates to x-ray imaging and spectroscopy in laser plasma experiments (invited). *Rev. Sci. Instrum*. **77**, 10E325.

Kawai, M., Kawamura, Y., & Toyoda, K. (1983). Discrete energy spectrum of an intense relativistic electron beam. *Phys. Lett*. **99A**, 387–390.

Kholodnaya, G., Ponomarev, D., Sazonov, R., & Remnev, G. (2014). Characteristics of pulsed plasma-chemical synthesis of silicon dioxide nanoparticles. *Radiat. Phys. Chem* **103**, 114–118.

Langmuir, I. (1913). The effect of space charge and residual gases on thermionic currents in high vacuum. *Phys. Rev*. **2**(6), 450–486.

Liu, Z.J., Le, X.Y., Jiang, X.L., & Han, L.J. (2005). Preparation of nanometer thin films with intense pulsed electron beam ablation. *Surf. Coat. Technol*. **193**, 325–328.

Mesyats, G.A. (1995). Ecton or electron avalanche from metal. *Phys. – Usp*. **38**(6), 567–591.

Rogers, D.W.O., Kawrakow, I., Seuntjens, J.P., & Walters, B.R.B. (2010). NRC user codes for EGSnrc. NRCC Report PIRS-702(revB).

Tanaka, K.A., Yabuuchi, T., Sato, T., Kodama, R., Kitagawa, Y., Takahashi, T., Ikeda, T., Honda, Y., & Okuda, S. (2005). Calibration of imaging plate for high energy electron spectrometer. *Rev. Sci. Instrum*. **76**, 013507.

Urazbahtina, L.R., Remnev, G.E., Goncharov, D.V., & Pushkarev, A.I. (2004). Radiolysis of methyl alcohol water solution by pulsed electron beam. *Russian-korean International Symp. on Science & Technology*, Vol. **2**, pp. 91–94.

Wohn, F.K., Clifford, J.R., Carlson, G.H., & Talbert, W.L. (1972). a plastic scintillation detector for beta-ray spectrum measurements. *Nucl. Instrum. Methods* **101**, 343–352.

Yu, X., Shen, J., Qu, M., Liu, W.B., Zhong, H.W., Zhang, J., Yan, S., Zhang, G.L., & Le, X.Y. (2015). Infrared imaging diagnostics for intense pulsed electron beam. *Rev. Sci. Instrum*. **86**, 083305.

Zhang, K.M., Zou, J.X., Bolle, B., & Grosdidier, T. (2013). Evolution of residual stress states in surface layers of an AISI D2 steel treated by low energy high current pulsed electron beam. *Vacuum* **87**, 60–68.

Zhang, X.D., Hao, S.Z., Li, X.N., Dong, C., & Grosdidier, T. (2011). Surface modification of pure titanium by pulsed electron beam. *Appl. Surf. Sci*. **257**(13), 5899–5902.

https://doi.org/10.1017/S0263034616000707 Published online by Cambridge University Press